Title page

Title. Heat release imaging in turbulent premixed methane-air flames close to blow-off

Authors. J. Kariuki[1], A. Dowlut[2], R. Yuan[1], R. Balachandran[2], E. Mastorakos[1]

[1]Hopkinson Laboratory, Engineering Department, University of Cambridge, CB2 1PZ, UK

[2]Department of Mechanical Engineering, University College London, WC1E 7JE, UK

Corresponding author. James Kariuki, email: jmk62@cam.ac.uk, Fax: +44 1223 332662

Colloqium. Turbulent flames.

Total length of paper. 6061 words

Method of determination. Method 1.

Main text: 4177 words

References: 385 words

Tables: 61 words

Table 1: 61 words

Figures and captions: 1438 words

Figure 1: 239 words

Figure 2: 241 words

Figure 3: 131 words

Figure 4: 199 words

Figure 5: 206 words

Figure 6: 194 words

Figure 7: 228 words

Other. Abstract length: 251 words.

The authors DO NOT wish to pay for color reproduction of figures.

Abstract

Estimates of the heat release (HR) of unconfined lean premixed methane-air flames stabilized on an axisymmetric bluff body have been measured for conditions increasingly closer to blow-off. Simultaneous imaging of OH- and CH_2O-PLIF was performed, and HR measurements obtained using the pixel-by-pixel multiplication of the OH- and CH_2O-PLIF images. Blow-off was approached by slowly reducing the fuel flow rate. At conditions far from blow-off, HR occurred along the shear layer, whereas at conditions near blow-off, HR was also observed inside the recirculation zone (RZ). Localised extinctions along the flame front were seen at conditions away from blow-off, and increased in frequency and size as blow-off was approached. At conditions near blow-off, HR was detected on the boundary of flame pockets inside the RZ which had detached from the fragmented flame at the attachment point. Regions void of OH in the RZ near blow-off were often seen to be filled with CH_2O. Regions void of both OH and CH_2O were also observed, but less often, indicating the presence of both preheated gases and fresh reactants inside the RZ. Such images do not show a connection with the annular air jet, implying the cold reactants entered the RZ from the top. HR was observed to increase as a function of the absolute value of flame front curvature for the near unity Lewis number flames investigated. The measurements reported here are useful for model validation and for exploring the changes in turbulent premixed flame structure as extinction is approached.

Key words. Turbulent premixed flames, OH-PLIF, CH_2O-PLIF, Heat release

1. Introduction

Detailed measurements of the reaction zone in turbulent flames are fundamental to the validation of combustion models. One useful diagnostic technique to achieve this is the simultaneous imaging of PLIF of OH and CH_2O. Early studies by Najm et al. [1] showed that the formyl radical HCO correlates very well with heat release rates in laminar premixed flames. However, obtaining sufficient signal intensities of LIF of HCO in laminar premixed flames have proved difficult due to insufficient LIF signal intensities [1]. Encouraged by the abundance of OH and CH_2O radicals in the flame front, and the dependence of HCO production to these radicals through the reaction $CH_2O + OH \rightarrow H2O + HCO$, Paul et al. [2] demonstrated that the profile of the pixel-by-pixel product of sequentially obtained LIF of OH and CH_2O images correlate well with heat release rates in premixed laminar flames.

The application of this diagnostic technique to turbulent reacting flows was demonstrated by Böckle et al. [3]. In their work, simultaneous LIF imaging of OH and CH_2O and Rayleigh temperature measurements showed that the overlapping regions of the LIF of OH and CH_2O profiles correlate with areas of intermediate temperatures in a turbulent Bunsen flame. In an additional experiment, sufficient signal of LIF of CH_2O was obtained in strongly turbulent swirling flames [3]. A broader distribution of CH_2O in the shear layer of the swirling flame than those observed in laminar and weaker turbulent flames was reported.

Balachandran et al. [4] and Ayoola et al. [5] applied the pixel-by-pixel product of OH and CH_2O PLIF to investigate the local flame structure and heat release effects in various lean premixed flames. Detailed observations on the local flame structure and effects of curvature on heat release [5] and on the flame response to inlet velocity oscillations [4] were reported, with the high spatial and temporal resolution offered by the technique allowing observations of flame annihilation events [4]. This technique has also been demonstrated to be a reliable indicator of heat release in non-premixed systems [6].

In contrast to flames far from extinction, whose behaviour is well summarised by Driscoll [7], flames close to blow-off have been studied little. Previous investigations of such flames were performed using fast OH-PLIF (5 kHz) to study changes in the flame structure at conditions approaching blow-off, and during the extinction transient [8, 9]. Lean premixed methane-air flames stabilized on a bluff body were studied. The flame front, tentatively defined by the edge of the LIF of OH profile, was shown to change from a continuous, smoothly wrinkled profile located along the shear

layer at conditions far from extinction, to become very contorted and disconnected at conditions near blow-off, with reaction moving inside the central recirculation region immediately downstream of the flame holder. Although the OH radical is commonly chosen in LIF experiments for planar characterization of flames, it is not an exact marker of the reaction zone as the OH radical is a relatively long-living intermediate at elevated temperatures and can be present in regions other than those of high reaction rates [10]. This hinders detailed investigation of the local flame structure, limiting the interpretation of the reaction zone behaviour of the near extinction flames [9]. The focus of the present work is to apply the pixel-by-pixel product of simultaneous PLIF of OH and CH_2O to investigate changes in the flame front structure and heat release of turbulent premixed flames approaching the lean extinction limit.

2. Experimental methods

2.1. Apparatus and flow conditions

The bluff body burner used was originally developed in Ref. [4] and is shown in Fig. 1. It consists of an inlet pipe of length 300 mm and inner diameter $D = 35$ mm mounted to a plenum with a flow straightener. A stainless steel conical bluff body (45° half-angle) with diameter $d = 25$ mm was mounted on a rod of diameter 6.35 mm, and concentrically fitted within the inlet pipe. The burner exit was profiled to a knife-edge and was open to the lab atmosphere. Methane and air at ambient conditions were premixed upstream. Air and fuel flow rates were controlled using Vögtlin Instruments mass flow controllers. The flame structure was investigated at four conditions, starting from a condition far from blow-off (A1), to a condition just prior to blow-off (A4). Table 1 details these conditions, which are identical to those studied in previous experimental work with fast (5 kHz) OH-PLIF [9]. Ref [9] should also be consulted for velocity and progress variable statistics and for regime identification of these flames.

2.2. OH and CH_2O PLIF

Two laser systems were used to simultaneously measure LIF OH and CH_2O across a planar section of the flame. The PLIF systems are shown schematically in Fig. 1. The OH-PLIF system used consists of a Fine Adjustments Pulsare-S tunable-dye laser pumped by a low repetition Litron Nd:YAG laser. Using a Rhodamine 6G dye solution, the tunable-dye laser produced a beam at 566 nm, which was then passed through a frequency doubler tuned to produce a beam near 283 nm to excite the $Q_1(6)$ line in the $A^1\Sigma$ - $X^2\Pi(1,0)$ band. The beam was then expanded into a

sheet of height and width of approximately 30 mm and 200 μm respectively using a combination of a plano-concave lens and a bi-convex lens. LIF of OH was captured using a TSI CCD camera, with 1376×1024 pixel resolution, coupled with a UV intensifier fitted with a Cerco 2178 UV lens (100F/2.8). A combination of WG305 and UG11 Schott glass filters were used to create a band pass filter (309-375 nm). The intensifier was gated at 200 ns at 5 Hz. Imaging was performed with an effective spatial resolution of approximately 25×25×200 μm per pixel, with 200 images recorded for each flame condition.

In the CH_2O-PLIF system, the output beam from a separate Litron Nd:YAG laser at 1064 nm was tripled to 355 nm to excite the $A^2A_1 \leftarrow X_1A^14_0^1$ pQ transition of CH_2O. The beam was then expanded into a sheet of height and width of approximately 25 mm and 300 μm respectively using a combination of a plano-concave lens and a bi-convex lens. LIF of CH_2O was captured using a TSI CCD camera, with 1376×1024 pixel resolution, coupled to a visible intensifier fitted with a Nikkon lens (50F/1.2). A combination of GG 395 and BG 40 filters were used to create a band pass filter (395-610 nm). The intensifier was gated at 200 ns at 5 Hz. Imaging was performed with an effective spatial resolution of approximately 25×25×300 μm per pixel, with 200 images recorded for each flame condition.

2.3. Image analysis

Following standard practices of processing simultaneously acquired PLIF signals [4, 6, 11], the raw OH and CH_2O PLIF images were initially corrected for the background noise, with a 3×3 median filter applied to improve the signal to noise ratio. The OH and CH_2O beam profiles were obtained by imaging the laser sheets from each dye laser passing through a cuvette filled with ethanol. A target image aligned in the PLIF measurement plane was imaged by both cameras. Identical reference points selected on the target image from each camera were used to define a transformation matrix relating the coordinate sets on both cameras. This was used to match the coordinate set on the OH camera to that on the CH_2O camera. One measure of goodness of fit of matching of the coordinate sets is the average deviation of the reference points of the matched images, which was found to be sub-pixel. The corrected and matched PLIF images were then resized using 2×2 binning, resulting in an effective spatial resolution of approximately 50×50×300 μm per pixel, following which the pixel-by-pixel multiplication of the two images was performed to estimate heat release.

3. Results and Discussion

3.1. Laminar flame simulations

Simulations of one-dimensional laminar unstrained freely propagating premixed methane-air flames were performed using the COSILAB software [12] to support interpretation of the PLIF images. The GRI-Mech 3.0 mechanism was used. Figure 2a shows the temperature, reaction rate (in arbitrary units) and molar fractions of O_2, CH_4, OH and CH_2O across a flame at $\phi = 0.75$. These results agree with the literature [1]. As expected, production of CH_2O starts in the preheat zone, peaks in the mid-temperature region of the flame, and is consumed at the high reaction rate regions. OH production begins after the production of CH_2O has started, and peaks in the high temperature post-flame region where all CH_2O has been consumed. In comparison with the profile of the reaction rate, the region of overlap of the OH and CH_2O profiles coincides with the location of peak heat release. Figure 2b shows the profile of the normalized product of OH with CH_2O plotted against the normalized reaction rate profile at equivalence ratios matching those investigated in the experiments. Good correlation is observed between the normalized OH×CH_2O and heat release profiles, with the peak of the OH×CH_2O profile matching the peak reaction rate well. These results are in agreement with data reported in the literature [13], and give confidence in using the pixel-by-pixel product of OH×CH_2O as a reliable indicator of heat release in the turbulent flames studied here. The width of the CH_2O profile was also estimated as the distance across the length of flame cross-section between the points where the profile rises above 5% of its peak value to where it falls below 5% of its peak value. The results are provided in Table 1, and show that the CH_2O region is slightly wider as ϕ is reduced. This widening mainly occurs at the tail of the CH_2O profile in the high reaction rate region, and is likely to result from the adverse effect of lower flame temperature on the reaction rate at more fuel-lean conditions, leading to a reduction in the consumption rate of CH_2O.

3.2. PLIF imaging

Figure 3 shows typical instantaneous images of the PLIF of OH and CH_2O. The edge of the OH LIF profile tentatively marks the boundary between the unburned and burned gas region of the flame, while the LIF of CH_2O is observed along the side of the annular jet of fresh reactants, near the flame front. The thin region of overlap of OH and CH_2O is shown by thick black lines superimposed on the OH image and marks, qualitatively, the region of heat release (HR). These observations agree well with previous results using the pixel-by-pixel product of PLIF of OH and CH_2O to investigate

heat release in turbulent premixed flames far from extinction [4, 5]. To supplement a discussion of the heat release imaging results, a summary of the geometry and aerodynamics of these flames from previous experimental work [9] is provided. The axisymmetric flame takes on a cylindrical shape at conditions away from blow-off, and the flame brush is located along the shear layer adjacent to the annular jet. The flame length is approximately $2.4d$, with a maximum width of approximately $1.6d$. d is the bluff body diameter. The region of hot recirculating gases is located immediately downstream of the flame holder and extends beyond a length of $1.6d$ from the bluff body. The location of the mean recirculation zone (RZ) is indicated in Fig. 1, where streamlines of the reacting flow at conditions far from extinction are presented together with the mean location of the flame edge. Typical values of the RMS axial and radial velocity inside the RZ are approximately $0.15U_b$ - $0.25U_b$ and $0.1U_b$ - $0.2U_b$ respectively. U_b is the bulk velocity at the annular exit of the burner. The RMS axial velocity reaches values of approximately $0.3U_b$ at the downstream parts of the shear layer, while the RMS radial velocity peaks downstream near the centreline of the RZ. As blow-off is approached, no significant changes are observed in the velocity field. However, the flame length shortens to approximately $1.6d$ and narrows to a maximum width of $1.1d$, as the downstream parts of the flame brush migrate from the shear layer to inside the recirculation zone. Typical values of the integral length scale local to the flame front are in the range of 2 - 4 mm and are comparable at both conditions away and close to blow-off. More details on the flame structure and turbulence characteristics are discussed in Ref. [9].

Examining the LIF profiles at condition A1, Fig. 3, the HR region located along the shear layer of the annular jet is observed to be wrinkled but unbroken. Occasionally, a vortex-like structure appears. In such instances, the width of CH_2O and HR are seen to increase locally in the region between the flame surfaces created. This behaviour has previously been reported in acoustically forced lean premixed flames [4], and was attributed to the vortex-like structures bringing reactants into the region between the flame surfaces, resulting in higher local HR at the point of focus. The thin region of HR along the shear layer at this condition is mostly continuous. However, breaks along this region are observed occasionally. This may indicate the presence of localised extinctions along the flame front, which is not clearly apparent from only observing the OH image. Localised extinctions could arise from the high aerodynamic stretch that the flame along the shear layer experiences, together with heat loss effects on the burnt side of the flame locally. The entrainment of cold air from the ambient may be significant, particularly for the unconfined flame studied here. However, no CH_2O is observed to penetrate the shear layer at this condition away from blow-off,

indicating sufficiently high reaction rates such that flame propagation of the flame attached to the bluff body closes these holes, and the stable burning flame is again achieved.

Figure 4 shows similar results at conditions A2 and A3. The HR region remains relatively thin and is located primarily along the shear layer. However stronger wrinkling of the HR region is observed. Breaks along the HR region increase in frequency and size, particularly at condition A3. Occasionally, as shown in Fig. 4, HR occurs at locations away from the shear layer, inside the recirculation zone (RZ) at its downstream parts. At these regions, CH_2O is observed at locations that are normally filled with OH at condition A1, indicating local quenching of the flame downstream. The fragmented structure of the HR region near the top of the RZ agrees with previous experimental work [9] with 5 kHz OH-PLIF. Significant fragmentation of the flame approaching blow-off was observed to begin at condition A3 at locations approximately 1.5 d downstream of the attachment point where the flame bends, crosses the shear layer, and closes across the RZ. The flame at this location was calculated to have a high Karlovitz number ($Ka = 0.25(u'/S_L)^2 Re_t^{-0.5}$, $Re_t = u'L_T/\nu$) relative to other parts of the flame front [9]. This indicates significant local straining of the reaction zone at the these regions, which together with volumetric heat loss effects could drive local extinctions. The surrounding high turbulence conditions may make re-ignition difficult, leading to the build up of CH_2O observed downstream prior to the re-establishment of the flame. Abundance of CH_2O with absence of OH in locally quenched regions of premixed methane-air jet flames at highly turbulent conditions was also observed in Ref [14], with flame quenching downstream also attributed to volumetric heat losses by entrained ambient air and high turbulence.

At conditions near blow-off, (A4 - Fig. 5), the flame is highly fragmented, and its shape changes significantly, both spatially and temporally. Local quenching of the flame downstream has intensified, and isolated regions of OH are seen inside the RZ. CH_2O is observed both downstream and in large regions inside the RZ, as seen in Figs. 5a and b. The laminar flame simulations showed only a small increase in the width of the CH_2O profile as ϕ was reduced from 0.75 to 0.64. The wide regions of CH_2O in the RZ are therefore not likely to result from widening of the CH_2O profile across the flame front, but indicate the presence of quenched or partially burned gases.

The presence of isolated OH pockets in the RZ prior to extinction of bluff body stabilized flames has been observed in the literature [9, 15, 16]. During the final stages of the blow-off event, at which the flame at the attachment point has been destroyed, these isolated pockets of OH are observed to survive in the RZ for a duration of the order of tens of milliseconds prior to total flame extinction [8, 9, 16]. In these studies, the presence of OH was used as an indicator of reaction, with

chemiluminescence and LIF imaging diagnostics applied. However, considering only the presence of OH is not sufficient to determine the presence of reaction within these flame pockets, or whether they comprise only short-lived post-reaction OH. However, the simultaneous PLIF measurements reported in this work show that these pockets of OH overlap with islands of CH_2O, indicating that reaction indeed takes place on the boundaries of these OH pockets. The contribution of these isolated flame structures to the total heat release of the flame validates their inclusion in the quantification of flame front metrics, such as FSD and curvature, done in Ref [9].

Occasionally, CH_2O is not observed in regions void of OH in the RZ, as seen in Fig. 5c. This may indicate that fresh reactants do penetrate inside the RZ. This in turn will facilitate the extinction of the shear layer flame. Previous work [8] using simultaneous OH^* and Mie scattering showed the entrainment of olive oil aerosol inside the RZ from the top for a stable flame at conditions very close to blow-off and during the extinction event. However, it was not possible to determine whether the entrained aerosol was fresh or preheated reactants. The PLIF measurements here show that both do occur, though entrainment of fresh reactants occurs less often. No connection is observed between the regions of cold reactants inside the RZ and the annular reactant jet. Also, the HR region is observed to be separated more often at the downstream than near the anchoring point. This implies that the cold reactants enter the RZ from the top following local extinction of the flame downstream, and not from small extinction holes at the sides of the RZ.

From these observations, some inferences on the flame structure can be made by referring to a hypothetical laminar flamelet structure that may be present at various locations at various instants. In region (i), Fig. 5a, fresh reactants in the shear layer can be thought of as impinging upon recirculated hot products; this would enable conditions to sustain a flame, leading to a continuous HR region. The break in the HR in region (ii), Fig. 5b, may arise from the fresh reactants impinging upon recirculated quenched or partially burned gases, resulting in local extinction. OH observed in region (iii), Fig. 5c, may probably be cooled combustion products at temperatures insufficient to establish a flame, quenching the flame locally. In region (iv), Fig. 5c, cold reactants in the shear layer may come in contact with entrained cold reactants in the RZ, and no reaction takes place. The wide regions of CH_2O in the RZ also indicates that low temperature combustion processes may take up a significant volume of the RZ at conditions near blow-off. It would be interesting to see if LES of premixed flames with appropriate models for finite rate chemistry and extinction can reproduce the large amounts of CH_2O present in the RZ close to blow-off.

Figure 6 shows the average LIF of OH and CH_2O profiles, and average HR, for conditions A1

and A4. The mean PLIF profiles agree with the observations from the instantaneous images. At condition A1, the RZ is filled with OH, and CH_2O is observed only along the shear layer. The mean flame brush, marked by the profile of the average HR, is observed to be relatively thin at the attachment point, where the HR intensity appears highest, and broadens further downstream. Similar results were observed by [4]. At condition A4, both OH and CH_2O are observed inside the RZ, where HR is also present.

The effect of flame front curvature on HR was also investigated. The flame front was defined by the edge of the OH LIF profile, and curvature values along the flame front were evaluated on the condition of detected HR. The flame front edge was first divided into 1 pixel length segments. A filter length of 5 points was chosen, and the edges filtered using a zero-phase digital filter. This doubled the filter order to 8 whilst providing no phase distortion. The flame front was then superimposed on the HR image, and the intensity of HR along a line normal to the flame tangent at each point was evaluated. The length of the normal line was selected to be 1 mm, corresponding to the typical width of the instantaneous HR region for flames A1 to A4. With 's' denoting the flame front length measured from a fixed origin on the filtered edge, values of curvature, on the condition of HR detected along the flame normal, were evaluated by calculating the first and second derivatives in the x and y directions along the edge with respect to s [17]. The first and second derivative curves were also filtered using the same zero-phase digital filter. Values of the local curvature were then calculated using $\kappa = \dot{x}\ddot{y} - \dot{y}\ddot{x}/(\dot{x}^2+\dot{y}^2)^{3/2}$, where $\dot{x}=dx/ds$ and $\ddot{x}=d^2x/ds^2$. With the flame front detected on the reactant side of the flame, the curvature is positive where the radius of curvature of the flame front is convex to the reactants, and negative where the radius of curvature is concave to the reactants. The OH laser sheet thickness, of approximately 200 μm, limits the curvature that can be resolved to approximately 5 mm^{-1}.

Figure 7a shows the probability density function (pdf)s of the local two-dimensional curvature for flames A1 to A4. The curvature values are multiplied by the corresponding laminar flame thickness δ_L at each experimental condition to obtain a non-dimensional measurement of flame front curvature. Values of δ_L are shown in Table 1. The distributions of $\kappa\delta_L$ are observed to be approximately Gaussian, and are symmetric about $\kappa = 0$. The pdfs are wider at conditions approaching blow-off. Similar results were reported for unforced premixed ethylene-air flames, where the flame front was defined from the edge of the HR profile [5]. The pdfs of $\kappa\delta_L$ also resemble distributions of curvature, not conditioned on HR, obtained at identical conditions with OH-PLIF [9]. Figure 7b shows bin averaged values of the average HR, with a bin width of $\kappa\delta_L = 0.1$ chosen.

To reduce error from random scatter, bin averages of HR were evaluated for bin sizes exceeding 200 points. HR is observed to increase as a function of the absolute value of flame front curvature, with a stronger increase in HR observed for positive curvatures and higher equivalence ratios. Numerical simulations performed by Chakraborty and Cant [18] showed that the reaction component of flame displacement speed for flames with unity Lewis number (Le) is negatively correlated with curvature on the fresh gas side of the flame while a positive correlation is observed on the burned gas side. The lean methane-air flames investigated here have Le values of approximately 0.98 [19]. However, two-dimensional estimates of flame front curvature are not likely to represent the true three-dimensional flame topology [20], and so interpretation of the correlation between HR and curvature presented in Fig. 7b should be viewed with caution.

4. Conclusions

Simultaneous imaging of PLIF of OH and CH_2O has been used to investigate changes in the flame structure and HR of stable, bluff body stabilized, turbulent premixed methane-air flames approaching the blow-off condition. Breaks occurring in the HR region at conditions far from blow-off indicated localised extinctions along the shear layer, which was not clearly apparent from the OH-PLIF signal. The HR region was shown to follow the key stages of the mean flame shape approaching blow-off: crossing the shear layer and entering the RZ. Possibly due to local quenching of the flame there, CH_2O was seen inside the RZ, i.e. in regions filled with OH at conditions further from blow-off. The HR region is observed to be disconnected more often at the downstream than near the anchoring point implying more extinctions there. At conditions near blow-off, HR occurs on the boundary of isolated flame pockets inside the RZ. Regions void of OH in the RZ were often filled with CH_2O. In some cases, regions void of both OH and CH_2O are seen in the RZ, indicating the entrainment of cold reactants. No connection is observed between the regions of cold reactants inside the RZ and the annular reactant jet, implying that the cold reactants enter the RZ from the top, supporting therefore the blow-off dynamics suggested previously based on fast OH-PLIF movies. Curvature measurements conditioned on HR showed no significant correlation. The data provided here can be used qualitatively for the validation of turbulent premixed flame models that include finite-rate chemistry effects.

5. Acknowledgements

Dr Balachandran and Mr Dowlut gratefully acknowledge support from EPSRC for research grant EP/G063788/1 and UCL/EPSRC Doctoral Training Account respectively that enabled measurement methods presented here. We also thank Prof. N. Swaminathan for useful discussions on heat release effects in premixed flames.

References

[1] H. N. Najm, P. H. Paul, C. J. Mueller, P. S. Wyckoff, Combust. Flame 113 (1998) 312–332.

[2] P. H. Paul, H. N. Najm, Proc. Combust. Inst. 27 (1998) 43–50.

[3] S. Böckle, J. Kazenwadel, T. Kunzelmann, D.-I. Shin, C. Schulz, J. Wolfrum, Proc. Combust. Inst. 28 (2000) 279–286.

[4] R. Balachandran, B. O. Ayoola, C. F. Kaminski, A. P. Dowling, E. Mastorakos, Combust. Flame 143 (2005) 37–55.

[5] B. O. Ayoola, R. Balachandran, J. H. Frank, E. Mastorakos, C. F. Kaminski, Combust. Flame 144 (2006) 1–16.

[6] R. L. Gordon, A. R. Masri, E. Mastorakos, Combust. Flame 155 (2008) 181–195.

[7] J. F. Driscoll, Prog. Energy Combust. Sci 34 (2008) 91–134.

[8] J. R. Dawson, R. L. Gordon, J. Kariuki, E. Mastorakos, A. R. Masri, M. Juddoo, Proc. Combust. Inst. 33 (2011) 1559–1566.

[9] J. Kariuki, J. R. Dawson, E. Mastorakos, Combust. Flame 159 (2012) 2589–2607.

[10] E. P. Hassel, S. Linow, Meas. Sci. Technol. 11 (2000).

[11] M. Röder, T. Dreier, C. Schulz, Proc. Combust. Inst. 34 (2013) 3549–3556.

[12] Rotexo-Softpredict-Cosilab, GmbH and Co. KG Bad Zweischenahn (Germany), Cosilab Collection, Version 3.0, 2009. Available from www.SoftPredict.com.

[13] H. N. Najm, O. M. Knio, P. H. Paul, P. S. Wyckoff, Combust. Sci. Tech. 140 (1998) 369–403.

[14] Z. S. Li, B. Li, Z. W. Sun, X. S. Bai, M. Aldén, Combust. Flame 157 (2010) 1087–1096.

[15] S. J. Shanbhogue, S. Husain, T. Lieuwen, Prog. Energy Combust. Sci 35 (2009) 98–120.

[16] S. Chaudhuri, S. Kostka, M. W. Renfro, B. M. Cetegen, Combust. Flame 157 (2010) 790–802.

[17] M. Z. Haq, C. G. W. Sheppard, R. Woolley, D. A. Greenhalgh, R. D. Lockett, Combust. Flame 131 (2002) 1–15.

[18] N. Chakraborty, R. S. Cant, Phys. Fluids 17 (2005).

[19] E. R. Hawkes, J. H. Chen, Combust. Flame 138 (2004) 242–258.

[20] R. S. M. Chrystie, I. S. Burns, J. Hult, C. F. Kaminski, Meas. Sci. Technol. 19 (2008).

Tables

Flame	U_b [m/s]	ϕ	δ_L [mm]	δ_{CH_2O} [mm]
A1	21.6	0.75	0.08	0.74
A2	21.5	0.70	0.10	0.81
A3	21.4	0.67	0.11	0.88
A4	21.4	0.64	0.13	0.97

Table 1: Summary of experimental conditions. δ_L is the laminar flame thickness (ν/S_L). δ_{CH_2O} is the width of the CH_2O profile calculated from simulations of 1-D laminar premixed flames.

Figures

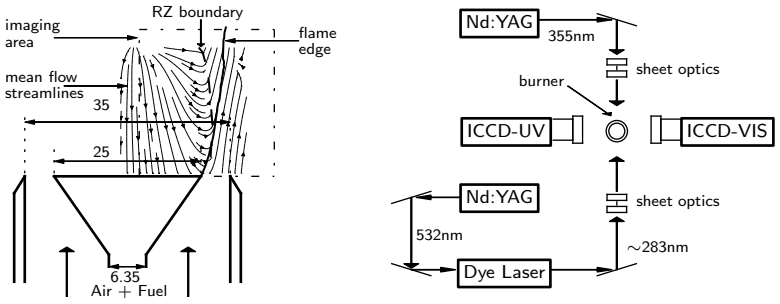

Figure 1: (Left) Schematic of the bluff body combustor. All dimensions in mm. (Right) Layout of the PLIF systems.

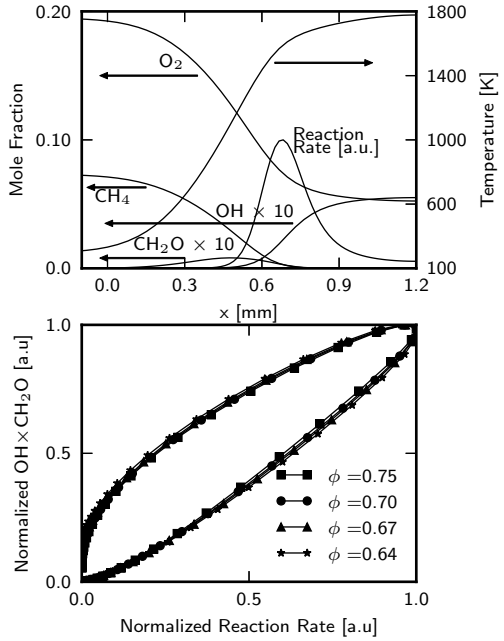

Figure 2: (a, Top) Calculated profiles of temperature, species molar fractions and the reaction rate for a laminar premixed flame at ϕ=0.75, and (b, Bottom) plots of normalized OH×CH_2O against the normalized reaction rate.

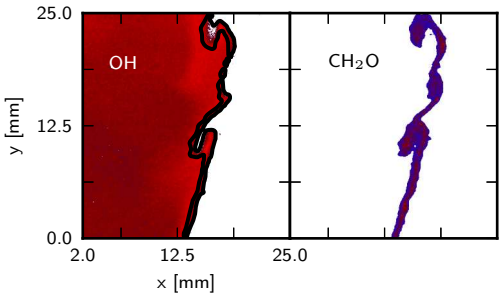

Figure 3: Instantaneous PLIF images for flame A1. The HR is shown by thick black lines superimposed on the OH image.

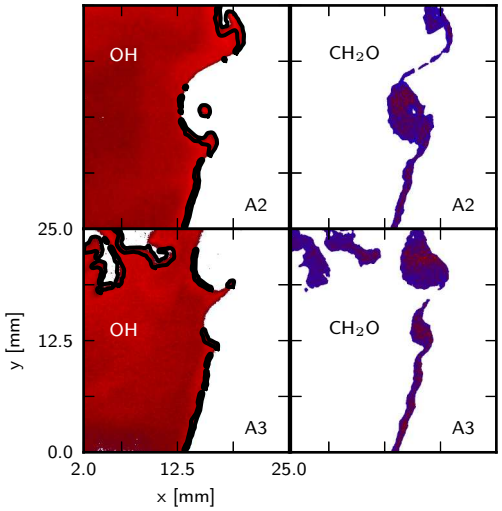

Figure 4: Instantaneous PLIF images for flame A2 and A3. The HR is shown by thick black lines superimposed on the OH image.

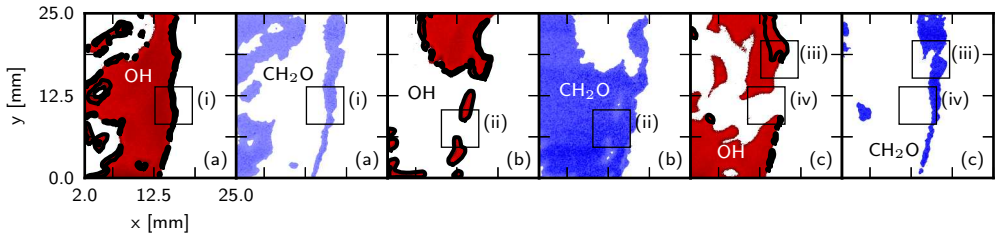

Figure 5: Instantaneous PLIF images for flame A4. The HR is shown by thick black lines superimposed on the OH image.

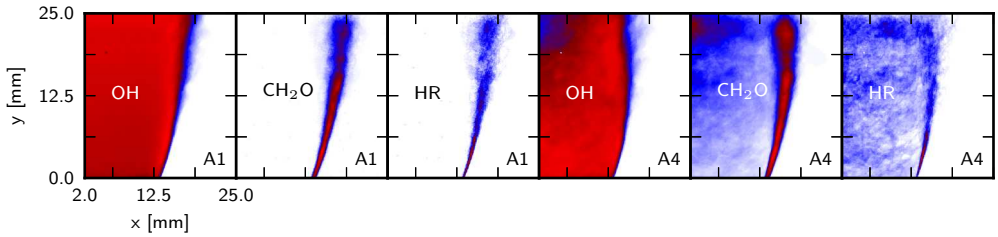

Figure 6: Images of the mean PLIF and HR.

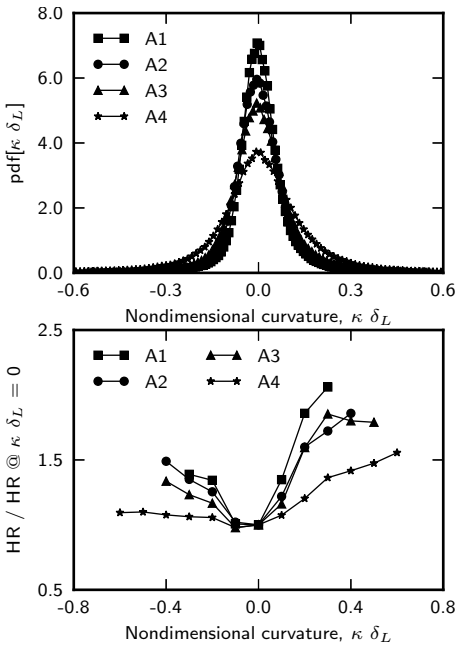

Figure 7: (a, Top) *pdf*s of curvature and (b, Bottom) plots of HR against curvature for flames A1 to A4.

Figure captions

Fig. 1: (Left) Schematic of the bluff body combustor. All dimensions in mm. (Right) Layout of the PLIF systems.

Fig. 2: (a, Top) Calculated profiles of temperature, species molar fractions and the reaction rate for a laminar premixed flame at ϕ=0.75, and (b, Bottom) plots of normalized OH×CH_2O against the normalized reaction rate.

Fig. 3: Instantaneous PLIF images for flame A1. The HR is shown by thick black lines superimposed on the OH image.

Fig. 4: Instantaneous PLIF images for flame A2 and A3. The HR is shown by thick black lines superimposed on the OH image.

Fig. 5: Instantaneous PLIF images for flame A4. The HR is shown by thick black lines superimposed on the OH image.

Fig. 6: Images of the mean PLIF and HR.

Fig. 7: (a, Top) *pdf*s of curvature and (b, Bottom) plots of HR against curvature for flames A1 to A4.